Geometric analysis of transient bursts

Hinke M. Osinga* and Krasimira T. Tsaneva-Atanasova†

Abstract

We consider the effect of a brief stimulation from the rest state of a minimal neuronal model with multiple time scales. Such transient dynamics brings out the intrisic bursting capabilities of the system. Our main goal is to show that a minimum of three dimensions is enough to generate spike-adding phenomena in transient responses, and that the onset of a new spike can be tracked using existing continuation packages. We take a geometric approach to illustrate how the underlying fast subsystem organises the spike adding in much the same way as for spike adding in periodic bursts, but the bifurcation analysis for spike onset is entirely different. By using a generic model, we further strengthen claims made in our earlier work that our numerical method for spike onset can be used for a broad class of systems.

Cellular responses are often characterised in terms of the sets of stimuli that increase or decrease their activity. The mathematical framework employed in studying such responses has put most emphasis on the stable states (point or periodic attractors) of a cellular system. In contrast, its transient (non-stationary) temporal behaviour has been given much less attention. Here we focus on computational ideas that allow us to study the transient dynamics of cellular systems. Indeed there are many situations in which the transient cellular behaviour manifests most of its functional significance, for example, while switching between different stable attractors. In order to understand better the relationship between response dynamics and system function we need to investigate transient dynamics and not just the asymptotically stable states. In this paper, we focus on the generation of bursts, consisting of one or more spikes, as a result of a brief external stimulus. We use a simple polynomial model of bursting to illustrate our analysis. In particular, we show the geometry of the mathematical framework used to generate a new spike and we discuss how to detect numerically the onset of a new spike by continuation of a two-point boundary value problem. This means that we can compute and present transitions between topologically different transient responses in a bifurcation diagram.

*Department of Mathematics, The University of Auckland, Private Bag 92019, Auckland 1142, New Zealand (h.m.osinga@auckland.ac.nz)

†Bristol Centre for Applied Nonlinear Mathematics, University of Bristol, University Walk, Bristol, BS8 1TR, United Kingdom (k.tsaneva-atanasova@bristol.ac.uk)

1 Introduction

The activity of a single neurone, recorded electrophysiologically in vitro, is usually characterised in terms of its response to a current injection of particular duration and/or wave form. Such approaches allow to verify experimentally the external and internal conditions, which affect intrinsic neuronal excitability. For certain sets of current-injection stimuli, such as long and short current injections, the firing activity of neurones may be enhanced, while for others there is no or little response [3, 4, 5]. Hence, neurones (and more generally, excitable cells) come with a specific intrinsic set of properties, which in turn characterises the set of stimuli or conditions to which the cell is most responsive. It is important to understand such intrinsic properties of neurones in order to identify when they may be malfunctioning. While variations in bursting rythms occur widely even for the same types of cells, our investigation shows how these may be linked to changes in the conditions internal to the cell; this means that any deviation from normal behaviour can be identified in terms of parameter variations that help point to the cause of the abnormal dynamics. In terms of mathematical modelling and theoretical analysis, relatively little attention has been given to the fact that the activity of many excitable cells may follow a certain time course during their response to a brief perturbation, such as a short current injection [4, 21, 22]. Here, we argue that theoretical analysis of the transient behaviour of excitable cells not only helps to shed light on biophysical and geometrical features of the generating dynamics, but it may also provide valuable insights into important functional processes as they evolve in time and pass through different stages.

Dynamical systems theory traditionally considers primarily asymptotic behaviour and explains long-term dynamics; however, this theory can also be used to study transient effects. For example, in the context of neuronal or cellular models, Rinzel considered singular limits of slow and fast time scales in the model and used bifurcation theory to classify periodic bursting patterns [25, 26]. This geometric approach in his work and that of others has led to an active research area in dynamical systems called geometric singular perturbation theory (GSPT); see also [6] for an overview. These ideas have been used successfully to study spike adding for periodic bursting behaviour. Pioneering work by Terman [29] provides a thorough analysis of transitions between bursting and tonic (continuous) spiking, and relates classical slow-fast analysis to the bifurcation analysis of the full system. Other studies [12, 13, 14] have focussed on the spike-adding mechanism directly. In general, this analysis demonstrates that the spike-adding mechanism is mediated by a pair of saddle-node bifurcations of periodic orbits of the full system; bursts with different numbers of spikes are, in fact, different periodic attractors of the full system that may co-exist [29]. Furthermore, in the case of periodic bursting, a spike-adding transition occurs over an exponentially small parameter interval [30]; see also [24].

Recently, we developed a biophysical model of a pyramidal CA1/3 excitable (neurone) cell [20] and analysed its transient response to a short current injection [21, 22]. In its minimal form the model is five dimensional, which we used to present a slow-fast analysis of its non-stationary behaviour. We showed how so-called slow manifolds of saddle type play an important role in generating additional spikes in

the transient response [21]. However, due to its five-dimensional nature, it was not possible to provide a full analysis of the geometric properties that organise the spike adding, and it remains unclear whether this type of transient response is a truly five-dimensional phenomenon. In [22], we discussed how to set up a two-point boundary value problem to detect the transient firing patterns in the system numerically. There, we also suggested that our proposed set-up is quite general and can be applied to other systems as well.

The goal of this paper is to provide a second case study of spike adding in a transient response. As can be expected from spike-adding transitions for periodic bursts, we are able to replicate the spike-adding behaviour for transient response as reported in [21, 22] by using a model with only one slow and two fast variables. We use the numerical method from [22] to compute a two-parameter bifurcation diagram that provides an overview of how transient bursting depends on parameters. Our model is a generic three-dimensional polynomial model that is based on the classical Hindmarsh-Rose system [16]; our polynomial formulation is such that the system can exhibit both square-wave and pseudo-plateau bursting, depending on the choice of parameters. An extensive bifurcation analysis for this system in the periodic bursting regime has been reported in [23, 31]. Here, we choose the parameters such that the system is quiescent unless a current is applied that perturbs it from its globally attracting equilibrium state; moreover, we ensure that the underlying structure is similar to the model for CA1/CA3 neurones used in [21, 22]. We present a geometric analysis of the effects of an applied current and provide a detailed numerical study of how the number of spikes in the response to such a perturbation changes as a result of interaction with the underlying slow manifolds of the system. The results in this paper not only confirm that spike adding as a transient phenomenon is essentially three dimensional, but also highlight the similarities with spike adding for periodic bursting, because the transients are organised by the same underlying geometric structure.

This paper is organised as follows. We introduce the model in Section 2 and provide a brief summary of the underlying dynamics that forms the basis for generating transient bursts. Here, we also explain briefly the numerical set-up of a two-point boundary value problem in the continuation package AUTO [8, 9] for the numerical detection of spike onsets. Section 3 illustrates how spikes are generated as a transient response and shows that the transition from an n-spike to an $(n+1)$-spike response occurs via a crossing of the stable manifold associated with the saddle-type slow manifold; we analyse this transition both for the one-to-two- and three-to-four-spike response. The numerical detection and continuation of the different spike onsets for our model are presented in Section 4. We compute the boundaries between regions with n-spike responses for $n = 1$ to 8 in a two-parameter bifurcation diagram. We end with a discussion in Section 5.

2 The three-dimensional polynomial model

We illustrate the geometry of spike adding for transient bursts using the three-dimensional model introduced in [23, 31] that is given by the following system of

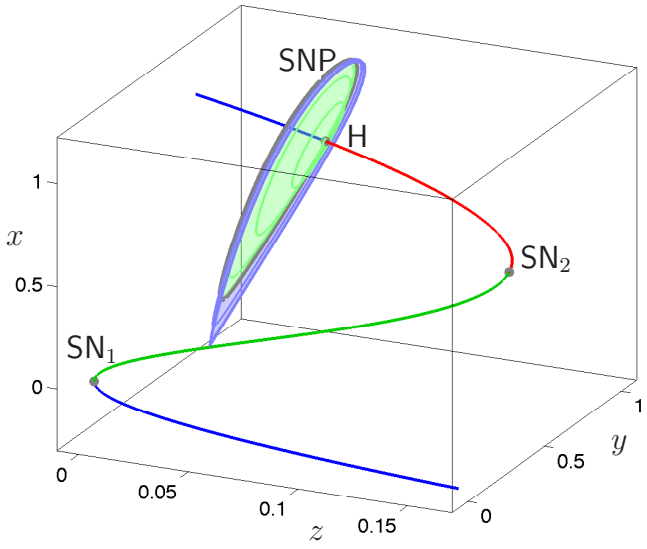

Figure 1: Bifurcation diagram plotted in (z, y, x)-space of system (1) in the singular limit $\varepsilon \to 0$. We used $b = 0.75$ and $h = 1.0$. The fast subsystem has a Z-shaped family of equilibria containing the saddle-node bifurcation points SN_1 and SN_2. The family also contains a subcritical Hopf bifurcation point H on the upper branch that gives rise to the family of periodic orbits that exhibits a saddle-node bifurcation of periodic orbits SNP before it ends in a homolinic bifurcation.

three ordinary differential equations

$$\left\{ \begin{array}{rcl} \dot{x} &=& s\,a\,x^3 - s\,x^2 - h\,y - b\,z, \\ \dot{y} &=& \phi(x^2 - y), \\ \dot{z} &=& \varepsilon(s\,a_1\,x + b_1 - k\,z). \end{array} \right. \tag{1}$$

The polynomial form of the equations makes it more amenable to algebraic analysis, but note the similarities with Hindmarsh-Rose systems [16, 27, 28]. Indeed, despite its simplicity, system (1) exhibits dynamics that are characteristic for neurophysiological models; the variable x acts like a membrane potential and y corresponds to a gating variable, while z plays the role of a slow variable representing, e.g., cytosolic Ca^{2+}. System (1) can produce many different periodic bursting patterns, including both square-wave and pseudo-plateau bursting [23, 31]. We choose the parameters such that the behaviour of system (1) resembles that exhibitied by the model for pyramidal neurones used in [21, 22]. That is, we fix $s = -2.0$, $a = 0.55$, $a_1 = -0.1$, $b_1 = 0.01$, and $k = 0.2$ with time-scale ratios $\phi = 1.0$ and $\varepsilon = 0.01$. The parameters b and h are our bifurcation parameters, which mimic the conductance parameter used in [22]; note that we had $h = 1$ in [23, 31]. The parameter h could represent the contribution of a delayed rectifier-like potassium current that is voltage dependent, while b controls the contribution of a slower (i.e. calcium sensitive) potassium current that depends on the slow variable z in the model.

System (1) offers the possibility of three different time scales, but spike adding for transient bursts can be generated using only two of them; by setting $\phi = 1$, the variables x and y change on a similar time scale that is faster than the time scale

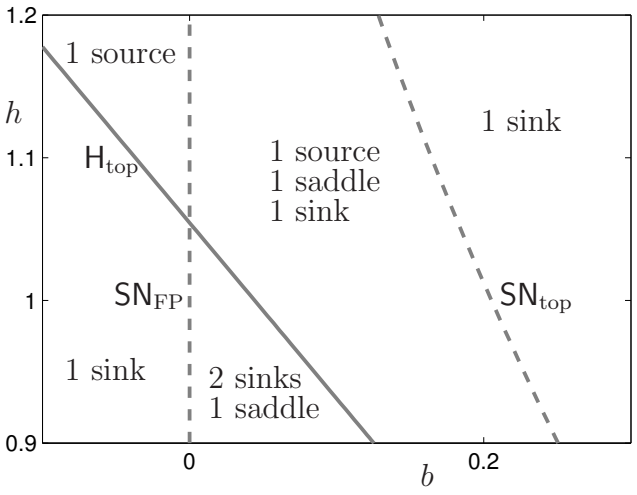

Figure 2: Bifurcation diagram in the (b, h)-plane near $b = 0$. Additional equilibria of system (1) exist due to fold bifurcations, labelled $\mathsf{SN}_{\mathrm{FP}}$ and $\mathsf{SN}_{\mathrm{top}}$, which can become stable due to a Hopf bifurcation, labelled $\mathsf{H}_{\mathrm{top}}$.

for z, with a ratio of $\varepsilon = 0.01$. The expected behaviour can then be explained by studying the system in the singular limit $\varepsilon \to 0$; the variable z effectively becomes a parameter in this limit and motion in the z-direction is frozen. Figure 1 shows the bifurcation diagram of the so-called fast subsystem using only the (x, y)-variables and treating z as the bifurcation parameter; here, z lies along a horizontal axis and x along the vertical axis. We fixed $b = 0.75$ and $h = 1.0$ here, but this choice is representative for the entire range of (b, h)-values considered in this paper. The fast subsystem has a Z-shaped family of equilibria that contain two saddle-node bifurcation points, denoted SN_1 and SN_2; the equations are formulated such that the left-most saddle-node bifurcation SN_1 is always at the origin. The equilibria on the lower branch, that is, for low values of x, are all stable; the middle branch in between SN_1 and SN_2 consists entirely of saddle equilibria; the equilibria on the upper branch, for high x-values, are stable if z is small, but they are repelling for z-values past a Hopf bifurcation point, denoted H. Our choice of parameters is such that H is subcritical, so that the emanating family of periodic orbits is unstable. This family becomes stable past a saddle-node bifurcation of periodic orbits, denoted SNP, and ends in a homoclinic bifurcation with the middle equilibrium branch.

Equilibria of the full three-dimensional system (1) lie on the Z-shaped family of equilibria of the fast subsystem. Their location is determined by the nullcline of z, which is given by the equation

$$z = \frac{s\, a_1\, x + b_1}{k},$$

and does not depend on y. We have chosen $a_1 = -0.1$, $b_1 = 0.01$ and $k = 0.2$ such that there exists a unique stable equilibrium FP on the lower branch. The location of FP depends on our bifurcation parameters b and h, but the effect is rather small in our region of interest $(b, h) \in [0, 3] \times [0.9, 1.1]$; in particular, FP is located on the lower branch provided $b > 0$. However, there exist other equilibria of system (1) if

b is close to 0, namely, when the z-nullcline also intersects the upper and middle branches of the Z-shaped family of equilibria of the fast subsystem. An overview of when this occurs is shown in Figure 2, which presents an enlarged view near $b = 0$. The equilibrium FP exists to the right of the curve $\mathsf{SN}_{\mathrm{FP}}$ at $b = 0$ in the (b, h)-plane. At $\mathsf{SN}_{\mathrm{FP}}$, it disappears in a fold bifurcation with a saddle equilibrium located on the middle branch that is created in another fold bifurcation curve, denoted $\mathsf{SN}_{\mathrm{top}}$. This other fold curve $\mathsf{SN}_{\mathrm{top}}$ also gives rise to an equilibrium on the upper branch, which is a source immediately to the left of $\mathsf{SN}_{\mathrm{top}}$, but becomes stable in a Hopf bifurcation, denoted $\mathsf{H}_{\mathrm{top}}$. A single equilibrium exists on the upper branch if $b < 0$, which is illustrated here for clarity. Inside our region of interest $(b, h) \in [0, 3] \times [0.9, 1.1]$, there exists a relatively small region of bistability, where both FP and the equilibrium on the upper branch are stable. However, the transient response is also influenced by the presence of unstable equilibria. Therefore, we consider only the region to the right of $\mathsf{SN}_{\mathrm{top}}$, in which FP is a unique and globally attracting equilibrium of system (1).

A transient response of system (1) is generated by applying a perturbation while the system is in its equilibrium state, that is, we assume that the initial condition is at FP before perturbation. The perturbation is generated for a finite time-duration of $T_{\mathrm{ON}} = 15$ via the modified x-equation

$$\dot{x} = s\, a\, x^3 - s\, x^2 - h\, y - b\, z + I_{\mathrm{app}}. \tag{2}$$

Here, $I_{\mathrm{app}} = 0.02$ is constant from $t = 0$ to $t = 15$ and reset (abruptly and discontinuously) to $I_{\mathrm{app}} = 0$ afterward. The effect of this perturbation is shown in Figure 3, where we used $b = 0.75$ and $h = 1.0$ as in Figure 1. Figure 3(a) shows the response overlayed on the bifurcation diagram of the fast subsystem; see also Figure 1. The time series of the x-coordinate over the time interval $[-50, 500]$ are shown in Figure 3(b); the segment of the response during which $I_{\mathrm{app}} = 0.02$ is highlighted in grey. We include a short segment $t \in [-50, 0)$ in the time series to highlight the fact that system (1) is at FP before the perturbation is applied.

We are interested in how the number of additional spikes after the given perturbation depends on the parameters b and h. To this end, we want to detect the onset of a new spike and consider curves of such spike onsets in the (b, h)-plane. The numerical detection of spike onsets can be done with the continuation package AUTO [8, 9] using a two-point boundary value problem (2PBVP) set-up; the precise details are described in [22]. We provide a brief overview of the main set-up in the remainder of this section and discuss the other steps as part of the results in Section 4.

2.1 Basic set-up of the 2PBVP in AUTO

The numerical detection and continuation of the onset of a new spike is explained in detail in [22], where it is used for a five-dimensional pyramidal neurone model. The computations are done using a two-point boundary value problem set-up, which is solved and continued with the software package AUTO [8, 9]. As explained in [22], the set-up is rather general and can be used for other models as well. Here, we briefly describe how to use the two-point boundary value problem set-up in the specific context of our model.

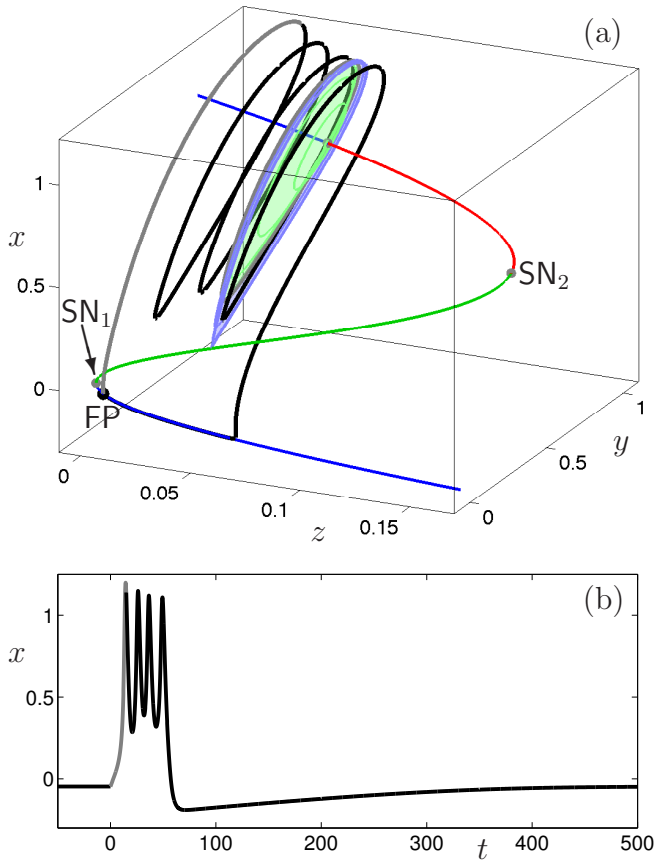

Figure 3: Transient response generated for system (1) with $b = 0.75$ and $h = 1.0$. A perturbation with amplitude $I_{\text{app}} = 0.02$ and duration $T_{\text{ON}} = 15$ takes the system away from its equilibrium FP (grey segment). The relaxation back to FP (black segment) exhibits three additional spikes before reaching FP. The response is shown in (z, y, x)- space in panel (a), with the underlying bifurcation diagram of the fast subsystem for reference; see also Figure 1. Panel (b) shows the corresponding time series for x with $t \in [-50, 500]$.

The main idea is to track the evolution of system (1) from $t = 0$, past the applied perturbation up to the maximum of the last spike; this last spike could have a very small amplitude, but it is defined as the last local maximum before the solution relaxes back to equilibrium. In the context of system (1), the maximum of a spike is in terms of x. Hence, we track the evolution from $t = 0$, with $I_{\text{app}} = 0.02$, up to $t = 15$ and then extend the orbit segment by integrating system (1), that is, $I_{\text{app}} = 0$, until the last local maximum in x is reached. The set-up in AUTO considers two orbit segments, one for the first perturbed segment with $I_{\text{app}} = 0.02$, and one for the second segment with $I_{\text{app}} = 0$. Hence, the problem is solved in a six-dimensional phase space with state vector $(\mathbf{u}_{\text{ON}}, \mathbf{u}_{\text{OFF}}) \in \mathbb{R}^6$, where $\mathbf{u}_{\text{ON}} = (x, y, z) \in \mathbb{R}^3$ represents the orbit segment integrated for a total integration time $T_{\text{ON}} = 15$ with an applied current $I_{\text{app}} = 0.02$, and $\mathbf{u}_{\text{OFF}} = (x, y, z) \in \mathbb{R}^3$ represents the orbit segment integrated for a total integration time T_{OFF} with no applied current, that is, $I_{\text{app}} = 0$. The value for T_{OFF} is defined implicitly as the time when the appropriate (local) maximum is achieved. As is customary in AUTO, the solution intervals for $\mathbf{u}_{\text{ON}}$ and $\mathbf{u}_{\text{OFF}}$ are scaled by T_{ON} and T_{OFF}, respectively, so that the orbit segment always starts at $t = 0$ and ends at $t = 1$. The boundary conditions of the two-point boundary value problem are chosen such that $\mathbf{u}_{\text{ON}}$ starts at FP and $\mathbf{u}_{\text{OFF}}$ starts at the point where $\mathbf{u}_{\text{ON}}$ ends; furthermore, we require that $\mathbf{u}_{\text{OFF}}$ ends at an extremum of x.

2.2 Computing spike-adding transitions

In order to find the spike-adding transitions, we initially vary a single parameter. Here, we begin our analysis by keeping $h = 1$ fixed and varying only b. As shown in Figure 3, for $b = 0.75$, system (1) produces a four-spike response to an applied current of strength $I_{\text{app}} = 0.02$ for a duration of $T_{\text{ON}} = 15$; the number of spikes in response to the same perturbation changes if we vary b. In order to capture these spike additions (or deletions), we consider the main two-point boundary value problem set-up, but define $T_{\text{OFF}} = 685$ fixed, instead of the implicit definition given in Section 2.1; see also [21]. This means that we consider orbit segments that respond to the given perturbation computed up to a total integration time of $T_{\text{ON}} + T_{\text{OFF}} = 700$; the total integration time is chosen long enough so that we can expect (approximate) convergence back to FP. We can continue this set-up in AUTO [8, 9], but note that there is no detection of the actual spike-adding events.

The results of the continuation in AUTO are shown in Figure 4(a) using the L_2 integral norm along orbit segments as a measure of the solution versus b. This norm is weighted with respect to the two integration times T_{ON} and T_{OFF} and computed over the full state space as follows:

$$\| (\mathbf{u}_{\text{ON}}, \mathbf{u}_{\text{OFF}}) \|_2 = \int_0^1 \sqrt{\| \mathbf{u}_{\text{ON}}(t) \|^2 + \| \mathbf{u}_{\text{OFF}}(t)) \|^2}\, dt,$$

where $\| \cdot \|$ denotes the usual Euclidean vector norm. Note that, effectively, a lot of weight is given to the T_{ON}-interval, while the size and shape of the solution $\mathbf{u}_{\text{ON}}(t)$ is actually relatively independent of b over such a short time interval; the location of FP hardly changes and the evolution with $I_{\text{app}} = 0.02$ has virtually the same effect

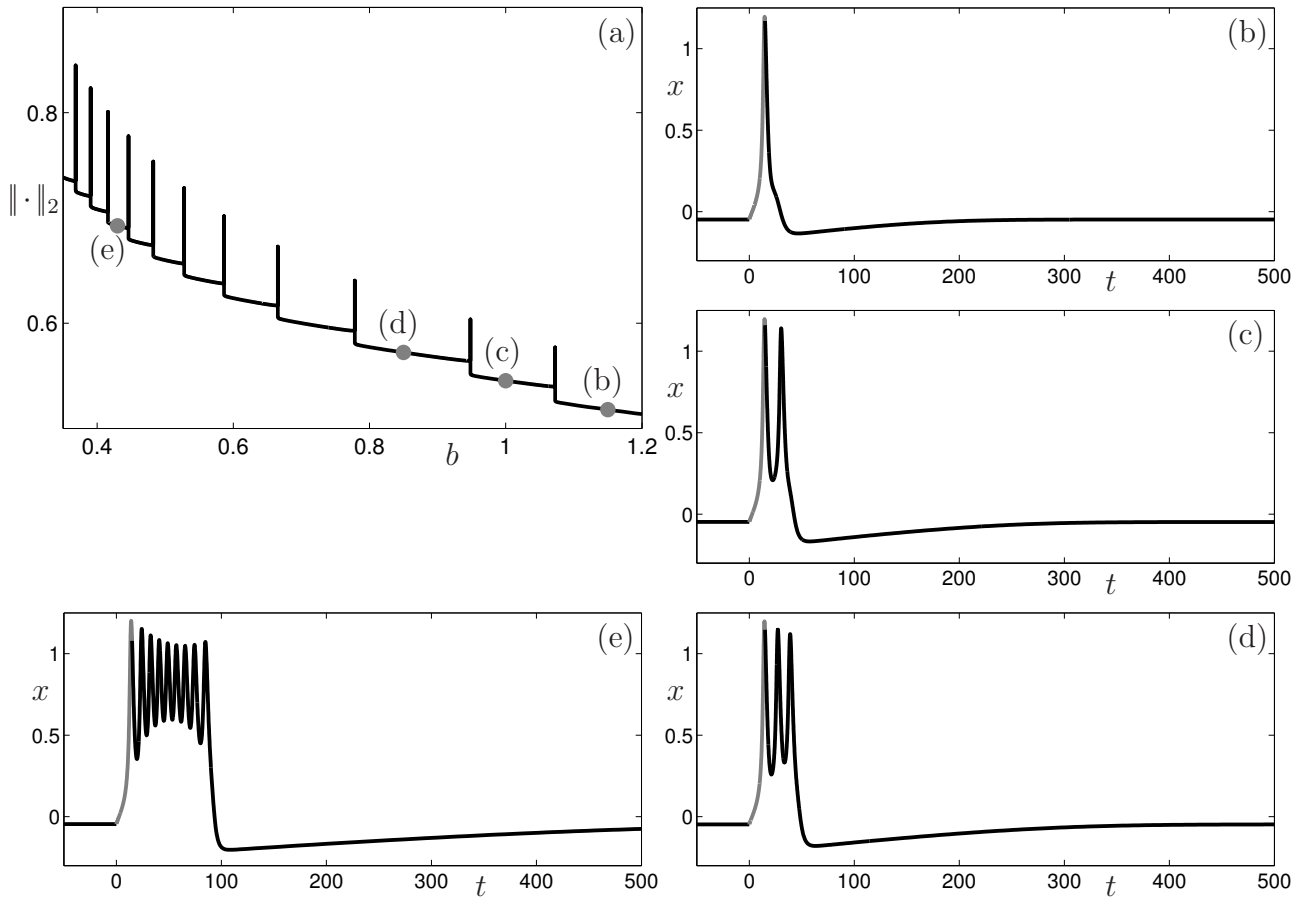

Figure 4: As b decreases, the response changes from 1 spike to more and more spikes, with each spike-adding transition characterised by a strong increase in the L_2 integral norm. Responses for $h = 1$ and $b = 1.15$ (one spike), $b = 1.0$ (two spikes), $b = 0.85$ (three spikes) and $b = 0.43$ (nine spikes) are highlighted and their corresponding time series for x are shown in panels (b)–(e), respectively.

for all b values considered. As a result, the contribution of $\mathbf{u}_{\mathrm{ON}}$ to the solution norm is almost constant and any variations are due to variations in the transient response represented by $\mathbf{u}_{\mathrm{OFF}}$. However, the contribution of $\mathbf{u}_{\mathrm{OFF}}$ is also almost constant from the moment that $\mathbf{u}_{\mathrm{OFF}}(t)$ (approximately) equals FP; hence, variations in the solution norm indicate a deviation from FP during the T_{OFF}-interval, which will be larger as the deviation lasts longer. As shown in Figure 4(a), the solution norm is slowly increasing as b decreases, but does so in a plateau-like fashion. Each plateau corresponds to a solution family with a particular number of spikes. We marked solutions on four plateaus and plot the time series for x in Figures 4(b)–(e); the labels in panel (a) indicate the panels in which the corresponding time series are shown. We do not plot the entire solution up to $t = 700$, but crop the time series at $t = 500$ for clarity; we also include a short time segment $-50 \leq t < 0$ to illustrate the location at FP before the perturbation is applied. The response of system (1) with $b = 1.15$ is shown in Figure 4(b) and shows a transient burst with only a single spike; this spike is generated while $I_{\mathrm{app}} = 0.02$ and the system immediately relaxes back to FP as soon as the applied current is turned off. The solution norm for this response is relatively small, because there is only one spike, which only exists, approximately, for $0 \leq t < 50$. The responses in Figures 4(c) and (d) are for $b = 1.0$ and $b = 0.85$, taken from the next two plateaus in panel (a), respectively; as expected, these responses contain two and three spikes, respectively, but note that the duration of these spikes is rather similar to the single spike in panel (a) and the total width of the burst creeps up only slowly. We invite the reader to verify that the response for $b = 0.43$ in Figure 4(e), based on its location in panel (a), is expected to contain nine spikes.

3 Spike onset along saddle-type slow manifold

We focus in this section on the transitions between the plateaus in Figure 4(a), where the number of spikes in the response increases by one as b decreases. Each time, from one plateau to the next, the L_2 integral norm increases abruptly and equally abruptly drops back down to a slightly higher value than before. Considering our observations in Figure 4, such an increase in norm must be due to the fact that the time interval during which the response is *not* at FP lengthens drastically for only an (extremely) short b-parameter interval. We made this same observation in [21] for a different model, which indicates that it may be characteristic for a spike-adding event.

Such abrupt variations in the L_2-integral norm are also present for periodic bursts; for example, see [24]. Spike adding for periodic bursts is mediated by saddle-node bifurcations of periodic orbits (SNP), which occur in pairs and generate an (exponentially) small parameter interval with three co-existing periodic solutions [12, 24, 30]. In contrast, the non-periodic nature of a transient response prohibits co-existence of solutions, which means that the continuation branch shown in Figure 4 is a function over b and the spike-adding mechanism cannot involve SNP bifurcations. However, it seems that the underlying geometric structure that organises the spike adding is the same as for periodic bursts: Each time a new spike is added, the response includes a segment during which the trajectory follows a slow

manifold of saddle type. In our context, this means that the response not only traces attracting states of the fast subsystem, but also includes a segment that traces the middle branch of saddle equilibria. We illustrate this behaviour using the transition from one to two spikes in Section 3.1 and consider the transition from three to four spikes in Section 3.2.

3.1 Transition from one- to two-spike response

The transition from a one- to a two-spike response at $h = 1$ occurs for $b \approx 1.07256$. In an exponentially small interval around this value of b, the L_2-integral norm varies dramatically; see Figure 4(a). Similar to what happens for periodic bursting patterns, the response in this exponentially small b-parameter interval includes a segment that traces a slow manifold of saddle type. This slow manifold of saddle type is associated with the saddle branch of the Z-shaped family of equilibria for the fast subsystem of (1). Let us introduce some notation. We denote by e_{M} the (middle) saddle branch of equilibria, that is, the z-dependent family of equilibria of the fast subsystem of (1) bounded by the fold points SN_1 and SN_2. The saddle slow manifold of the full system (1) is denoted $\mathcal{S}_{\mathrm{M}}$. The manifold $\mathcal{S}_{\mathrm{M}}$ is well approximated by e_{M} (away from the folds SN_1 and SN_2), because it lies $O(\varepsilon)$ close to it [7, 10]; in fact, in the limit $\lim_{\varepsilon\to 0} \mathcal{S}_{\mathrm{M}} = e_{\mathrm{M}}$.

The geometric picture that we have in mind is as follows: Each saddle equilibrium on e_{M} has a one-dimensional stable manifold that acts as a separatrix in the fast (x, y)-subspace. Together, these one-dimensional stable manifolds form a z-dependent two-dimensional surface, denoted $W^s(e_{\mathrm{M}})$, which also acts as a separatrix in the full (x, y, z)-space because there is no flow in the z-direction for the fast subsystem of (1). The fast subsystem provides information about the nature of the transient response by describing what happens if z would not change: as soon as the applied current is turned off, the response has reached a state associated with a particular z-value; the fast subsystem predicts what happens based on the state at this value of z. A spike will follow if this state lies in the basin of attraction of the equilibrium on the upper branch. Otherwise, the system relaxes back to the fixed point FP, which is represented by attraction to the equilibrium on the lower branch. The fast subsystem predicts that a spike-adding transition occurs when the response lies exactly on the basin boundary $W^s(e_{\mathrm{M}})$: namely, in this case, the fast subsystem cannot decide whether to predict a spike or relaxation to FP.

Unfortunately, the invariant manifolds of the fast subsystem are not invariant manifolds of the full three-dimensional system (1). The true nature of events involves the saddle slow manifold $\mathcal{S}_{\mathrm{M}}$ and its associated stable manifold, denoted $\mathcal{F}(\mathcal{S}_{\mathrm{M}})$, which are only finite-time invariant manifolds; due to this finite-time nature, $\mathcal{F}(\mathcal{S}_{\mathrm{M}})$ does not separate phase space in the same way as $W^s(e_{\mathrm{M}})$ and the full system (1) eventually always relaxes back to FP. Let us define $\mathcal{S}_{\mathrm{M}}$ and $\mathcal{F}(\mathcal{S}_{\mathrm{M}})$ more precisely. We think of $\mathcal{S}_{\mathrm{M}}$ as the finite-time invariant manifold that exists until the fast time scales take over. More precisely, $\mathcal{S}_{\mathrm{M}}$ is an orbit segment, contained in a trajectory, that remains $O(\varepsilon)$ close to e_{M} for $O(1)$ time; see also [6] for further details. The start and end points of $\mathcal{S}_{\mathrm{M}}$ are ill defined: one could start and end $O(\varepsilon)$ close to almost any point on e_{M} as long as the slow epoch lasts $O(1)$ time. Hence, $\mathcal{S}_{\mathrm{M}}$ is not

unique, though it is often defined as the *maximal* orbit segment, that is, the one that remains $O(\varepsilon)$ close to e_{M} for the longest $O(1)$ time. Note that all possible choices for $\mathcal{S}_{\mathrm{M}}$ lie exponentially close together. Each such $\mathcal{S}_{\mathrm{M}}$ has a finite-time stable manifold $\mathcal{F}(\mathcal{S}_{\mathrm{M}})$. Locally, in a tubular neighbourhood of $\mathcal{S}_{\mathrm{M}}$, this stable manifold is uniquely defined as the manifold tangent at $\mathcal{S}_{\mathrm{M}}$ to the linear stable normal bundle of $\mathcal{S}_{\mathrm{M}}$; the linear stable normal bundle of a finite-time manifold is again not unique, but all possible choices lie exponentially close together. Outside the tubular neighbourhood of $\mathcal{S}_{\mathrm{M}}$, the finite-time stable manifold $\mathcal{F}(\mathcal{S}_{\mathrm{M}})$ can be viewed as a family of fast orbit segments. To the best of our knowlege, there is no numerical method to compute $\mathcal{F}(\mathcal{S}_{\mathrm{M}})$; we refer to [14] for ideas on how one might go about this. We use $W^s(e_{\mathrm{M}})$ as an approximation of $\mathcal{F}(\mathcal{S}_{\mathrm{M}})$, because in the limit

$$\lim_{\varepsilon \to 0} \mathcal{F}(\mathcal{S}_{\mathrm{M}}) = W^s(e_{\mathrm{M}}).$$

We remark here that the infinite-time invariant manifold $W^s(e_{\mathrm{M}})$ of the fast subsystem is a good approximation of the finite-time invariant manifold $\mathcal{F}(\mathcal{S}_{\mathrm{M}})$ of the full system (1) only locally near $\mathcal{S}_{\mathrm{M}}$, because z should not drift too much before reaching $\mathcal{S}_{\mathrm{M}}$.

Let us now illustrate the geometry behind the transition from one to two spikes. We fix $h = 1$ and $b = 1.07256$ and consider the Z-shaped family of equilibria the fast subsystem; as for $b = 0.75$ in Figure 1, we also compute the family of periodic orbits emanating from the Hopf bifurcation on the upper branch. The saddle branch e_{M} of the Z-shaped family lies in between the saddle-node bifurcation points SN_1 and SN_2, and contains a homoclinic point HC at which the family of periodic orbits ends. We focus on the stable manifolds associated with the saddle equilibria in between SN_1, at $z = 0$, and HC, at $z \approx 0.03433$, that is, we compute only a subset of $W^s(e_{\mathrm{M}})$. We select 11 z-values uniformly distributed in the interval $[0.003, 0.033]$ and consider the associated saddle equibrilia on e_{M}. For each saddle equilibrium, we compute its stable manifold as the two orbit segments that end at distance 10^{-6} from the equilibrium along the positive and negative directions of the stable eigenvector; the computation is done by integration backward in time from these two points until the orbit segments reached the plane $\{x = -0.5\}$.

Figure 5 shows these invariant manifolds of the fast subsystem from two different viewpoints in panels (a) and (b). The Z-shaped branch of equilibria and the family of periodic orbits emanating from the Hopf bifurcation is similar to the case for $b = 0.75$ shown in Figure 1. In Figure 5, we also include the part of $W^s(e_{\mathrm{M}})$ that is associated with the selected equilibria on e_{M}, which is rendered as the two-dimensional light-blue surface and labelled $W^s(e_{\mathrm{M}})$ for convenience. The two view points illustrate how one side (the negative side) of $W^s(e_{\mathrm{M}})$, goes straight down (in backward time) to the plane $\{x = -0.5\}$, while the other (positive) side of $W^s(e_{\mathrm{M}})$ folds around the upper branch and the family of periodic orbits, before it also goes down to the plane $\{x = -0.5\}$. Overlayed in black is the transient response that we consider to be the one at the moment of onset of the second spike; as in Figure 3 the segment of the response during which $I_{\mathrm{app}} = 0.02$ is highlighted in grey. The overlayed response has the longest time interval during which it is not (approximately) at FP; we can see this in the phase portraits in (x, y, z)-space shown in Figures 5(a) and (b), because the orbit follows e_{M} all the way up to SN_2. The delayed relaxation back to FP can

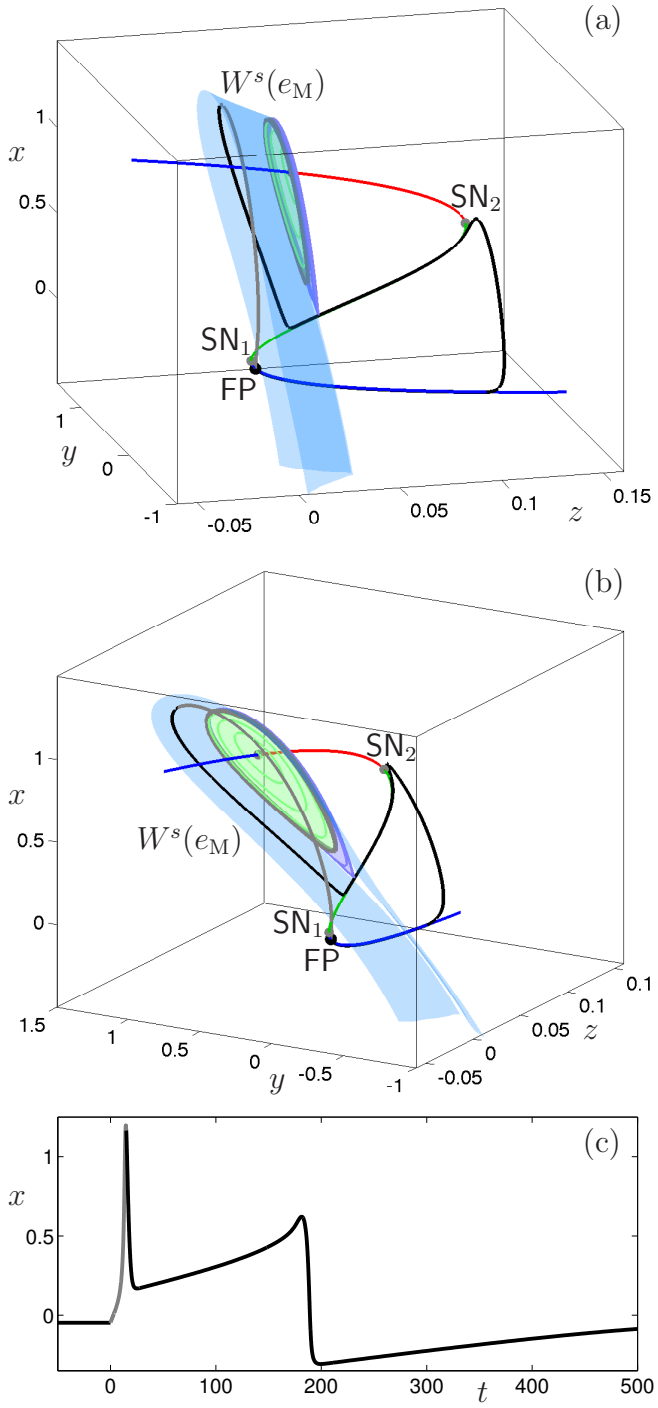

Figure 5: Two viewpoints in panels (a) and (b) of the transient response at the onset from one to two spikes; we also show the bifurcation diagram of the fast subsystem, along with a subset of the family $W^s(e_{\mathrm{M}})$ of stable manifolds associated with saddle equilibria on the middle branch e_{M} in between SN_1 and the homoclinic bifurcation (not labelled). The response for $b \approx 1.07256$ traces e_{M} up to the fold point at SN_2; panel (c) shows the corresponding time series for x with $t \in [-50, 500]$.

also clearly be seen in the time series in Figure 5(c), which shows the x-coordinate of the response on the time interval $[-50, 500]$ in panel (c); it takes until $t \approx 181.8$ before the response exhibits a rapid drop to the equilibrium value at $x \approx -0.0481$.

Figure 5 illustrates that the perturbation due to a short current application ($I_{\text{app}} = 0.02$), for this special value of $b \approx 1.07256$, has the effect that the overlayed transient response lands on $\mathcal{F}(\mathcal{S}_{\text{M}})$. Indeed, for the transition from one to two spikes, $W^s(e_{\text{M}})$ is a very good approximation of $\mathcal{F}(\mathcal{S}_{\text{M}})$, because the segment that starts at the moment when the applied current is switched off ($I_{\text{app}} = 0$) follows $W^s(e_{\text{M}})$ despite the slow drift in z and clearly converges to e_{M}, after which it traces e_{M} until it almost reaches SN_2. Before this transition, that is, for slightly larger values of b, the transient response lands 'behind' $W^s(e_{\text{M}})$ with respect to the viewpoint in Figure 5(a); this region corresponds to the basins of attraction of equilibria on the lower branch and the fast subsystem predicts relaxation back to FP. For slightly smaller values of b, after the transition, the transient response lands 'in between' the first local part and the folded part of $W^s(e_{\text{M}})$; this region corresponds to the basins of attraction of equilibria on the upper branch and the fast subsystem predicts a spike.

3.2 Transition from three- to four-spike response

Let us now consider the transition from a three- to a four-spike response, which occurs at $b \approx 0.778355$ if $h = 1$; see the dramatic variation of the L_2-integral norm at this value in Figure 4(a). As in Section 3.1, we fix $h = 1$ and $b = 0.778355$ and consider the Z-shaped family of equilibria along with the family of periodic orbits that emanates from the Hopf bifurcation. In fact, these invariant manifolds of the fast subsystem are very similar to the ones shown for $b = 1.07256$ in Section 3.1 or for $b = 0.75$ in Section 2; they share the same bifurcations and stability properties. The branch e_{M} of saddle equilibria lies again in between the saddle-node bifurcation points SN_1 and SN_2, and it also contains a homoclinic point HC at which the family of periodic orbits ends. As for the case with $b = 1.07256$, we select a range of z-coordinates for which we compute the stable manifolds of the corresponding saddle equilibria. Each manifolds is again computed by backward integration from the two points at distance 10^{-6} from the equilibrium along the positive and negative directions of the stable eigenvector. However, for the transition from three to four spikes, we also consider z-values past HC, which occurs at $z \approx 0.0473$. We compute stable manifolds to the left and to the right of the homoclinic bifurcation by selecting 11 z-values uniformly distributed in the interval $[0.003, 0.047]$ and 3 z-values uniformly distributed in the interval $[0.0476, 0.0564]$, respectively. The stable manifolds for saddle equilibria in between SN_1 and HC are computed up to their intersection with the plane $\{x = -0.5\}$. The stable manifolds for the saddle equilibria to the right of HC, for $z \in [0.0476, 0.0564]$, are of a different nature: the negative side is similar to the negative side for $z \in [0.003, 0.0473]$ and the combined family forms a smooth manifold that is part of $W^s(e_{\text{M}})$; the positive side for each $z \in [0.0476, 0.0564]$, on the other hand, spirals around the unstable (source) equilibrium on the upper branch that corresponds to the same z-vale, and accumulates (backward in time) onto this equilibrium. The positive sides of the family to the left of HC fold only once and

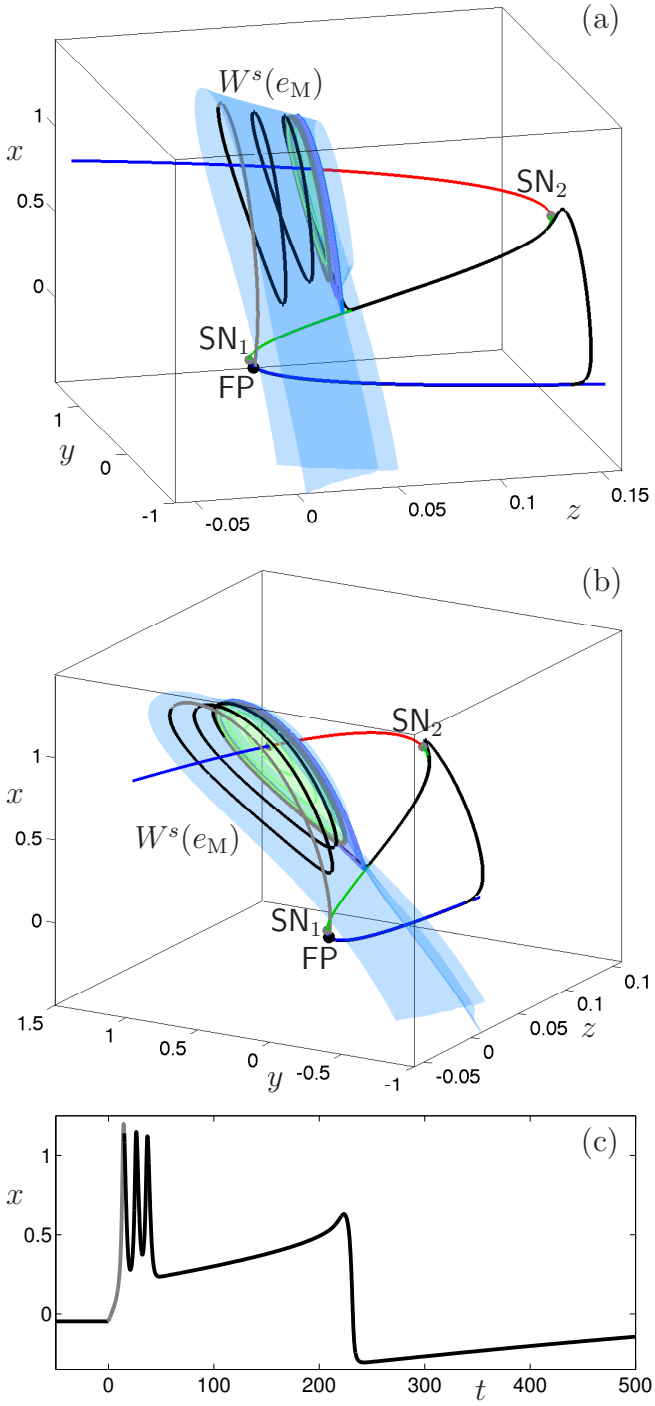

Figure 6: Two viewpoints in panels (a) and (b) of the transient response at the onset from three to four spikes; we also show the bifurcation diagram of the fast subsystem, along with a subset of the family $W^s(e_{\mathrm{M}})$ of stable manifolds associated with saddle equilibria on the middle branch e_{M} in between SN_1 and just past the homoclinic bifurcation (not labelled). The response for $b \approx 0.778355$ traces e_{M} up to the fold point at SN_2; panel (c) shows the corresponding time series for x with $t \in [-50, 500]$.

accumulate onto the negative sides of manifolds in $W^s(e_{\rm M})$ that correspond to the same z-value. The homoclinic orbit itself separates the two families and is the only manifold with finite arclength; In order to render the surface $W^s(e_{\rm M})$ from these different families, we compute the spiralling positive sides up to arclength 2.6.

Figure 6 shows the Z-shaped critical manifold and the family of periodic orbits from two different viewpoints in panels (a) and (b), together with the part of $W^s(e_{\rm M})$ that is associated with the selected saddle equilibria on $e_{\rm M}$. The geometric structure is qualitatively very similar to that shown in Figure 5, which did not show the stable manifolds to the right of HC. Figure 6 also shows, overlayed in black, the transient response with the longest time interval during which it is not (approximately) at FP; as before, the segment during which $I_{\rm app} = 0.02$ is highlighted in grey. As was the case for $b = 1.07256$, the transient response follows $e_{\rm M}$ all the way up to SN_2, and only relaxes back to FP at $t \approx 223.6$; see Figure 6(c).

The interpretation of Figure 6 is not as straightforward as for the one- to two-spike transition shown in Figure 5, because $W^s(e_{\rm M})$ is not a good *global* approximation of $\mathcal{F}(\mathcal{S}_{\rm M})$. The 'convergence' to $\mathcal{S}_{\rm M}$ after the short current application involves a drift in z over too large a z-interval and $W^s(e_{\rm M})$ cannot be used as an approximation of $\mathcal{F}(\mathcal{S}_{\rm M})$ immediately after the applied current is switched off. This means that we should not expect that the transient response follows $W^s(e_{\rm M})$ from the beginning. As shown in Figure 6, as soon as the applied current is switched off, the transient response lies very close to $W^s(e_{\rm M})$, 'in between' the first local part and the folded part of $W^s(e_{\rm M})$. Hence, the fast subsystem predicts a spike. If we follow the trajectory to the maximum of this second spike, the transient response lies again in between the first local part and the folded part of $W^s(e_{\rm M})$, so that a third spike is predicted. The fast orbit segment past this third spike lies approximately on the computed family of stable manifolds in $W^s(e_{\rm M})$. Despite the slow drift in z, this last segment of the transient response does follow $W^s(e_{\rm M})$, and clearly converges to, and subsequently traces $e_{\rm M}$ until it almost reaches SN_2.

The two transitions, from one to two spikes as described in Section 3.1, and from three to four spikes as described in this section, are representative for the other transitions observed in system (1), and can be seen as the general scenario for a transition from n to $n+1$ spikes in a transient response.

4 Two-parameter curves of spike onsets

As illustrated in Section 3, the onset of a new spike is accompanied by a dramatic increase in $T_{\rm OFF}$, due to the fact that the last local maximum occurs at the end of a very slow epoch, initiated by a convergence to and subsequent tracking of a saddle-unstable slow manifold. We view this as characteristic behaviour and define the moment of spike onset as the parameter value that corresponds to a solution pair $(\mathbf{u}_{\rm ON}, \mathbf{u}_{\rm OFF})$ for which $T_{\rm OFF}$ is (locally) maximal; see also [21]. Since $T_{\rm OFF}$ is possibly unbounded, we argue in [22] that a (local) maximum of $T_{\rm OFF}$ must be accompanied by a local extremum of the slow variable(s). For system (1), the slow variable z will reach a (local) maximum each time when $T_{\rm OFF}$ is (locally) maximal. Therefore, numerically, we detect the onset of a spike as a fold bifurcation with respect to the z-coordinate at the end point $\mathbf{u}_{\rm OFF}(1)$; we refer to [22] for the precise details on how

to set this up in AUTO.

The first detection of the onset of a new spike is done using a one-parameter continuation, say, by varying b, while h remains fixed. As an illustration, let us assume that we want to detect the onset of the second spike; the generalisation to onset of the n-th spike is straightforward. We fix $h = 1$ and start the continuation with a first solution pair $(\mathbf{u}_{\rm ON}, \mathbf{u}_{\rm OFF})$ at $b = 1$ for which the response consists of two spikes before it relaxes back to FP. As described in Section 2.1, $(\mathbf{u}_{\rm ON}, \mathbf{u}_{\rm OFF})$ is only generated up to the second local maximum in x. We then run the continuation by increasing b towards the moment of spike onset and simultaneously monitoring the z-coordinate at the end point $\mathbf{u}_{\rm OFF}(1)$, which we denote by $z_{\rm end}$. The results are illustrated in Figure 7(a) with a waterfall diagram showing the time series of x; here, we again included a first segment of the time series with $t \in [-50, 0)$ to highlight that $\mathbf{u}_{\rm ON}(0) = \mathsf{FP}$. The waterfall diagram is drawn with respect to the index N of the continuation steps taken, which provides some measure of the variation in the L_2-integral norm between successive solutions of the two-point BVP. Observe that each time series stops at an extremum of x, which is the second local maximum at the start of the continuation, but turns into a local minimum as the continuation progresses past the point of spike onset.

For the first solution pair $(\mathbf{u}_{\rm ON}, \mathbf{u}_{\rm OFF})$ at $(b, h) = (1, 1)$, the integration time of the second orbit segment satisfies $T_{\rm OFF} \approx 15.4078$, and for the last solution pair in this continuation it is $T_{\rm OFF} \approx 11.5609$. However, during this transition from local maximum to local minimum, the integration time of the second orbit segment reaches a maximum of $T_{\rm OFF} \approx 166.8252$; compare also the time series in Figure 5(c), for which the fast drop back to FP occurs at $T_{\rm ON} + T_{\rm OFF} \approx 181.8$. This solution pair with the largest value for $T_{\rm OFF}$ is highlighed as a slightly thicker curve in Figure 7(a). The continuation run in AUTO also detects a fold, denoted LP, at precisely this solution pair; hence, the (local) maximum in $T_{\rm OFF}$ coincides with a (local) maximum in $z_{\rm end}$.

Figure 7(b) illustrates how b varies during the continuation. We show both $T_{\rm OFF}$ (left axis) and b (right axis) in the same plot with the index N of the continuation steps on the horizontal axis; the moment of spike onset is indicated by the vertical dotted line labelled LP. Note that b initially increases, but then levels off before the spike onset and remains approximately constant at $b \approx 1.072563$ for most of the continuation run. Indeed, the increase in b during the spike-adding transition is exponentially small. Figure 7(c) shows both $T_{\rm OFF}$ (left axis) and $z_{\rm end}$ (right axis) in the same plot as functions of N; the moment of spike onset is again indicated as in panel (b). Note that $T_{\rm OFF}$ and $z_{\rm end}$ are both maximal at the moment of spike onset.

We generate an entire set of spike onsets for the nth spike with $n = 2, 3, \ldots, 9$ by following the above set-up. That is, for each n we select a suitable value for b, with $h = 1$ fixed, such that the transient response exhibits a total of n additional spikes, ending at the maximum (in x) of the nth spike. We then vary b and detect the moment when $z_{\rm end}$ is maximal as a fold bifurcation with AUTO [8, 9]. These fold points can subsequently be continued in two parameters. Figure 8 shows the bifurcation diagram of spike onsets in the (b, h)-plane using a dark-to-light colour gradient with increasing numbers of spikes. Here b ranges from 0.1 to 3 and h from 0.9 to 1.1. We halt the continuation at $b = 0.1$, because all curves have crossed

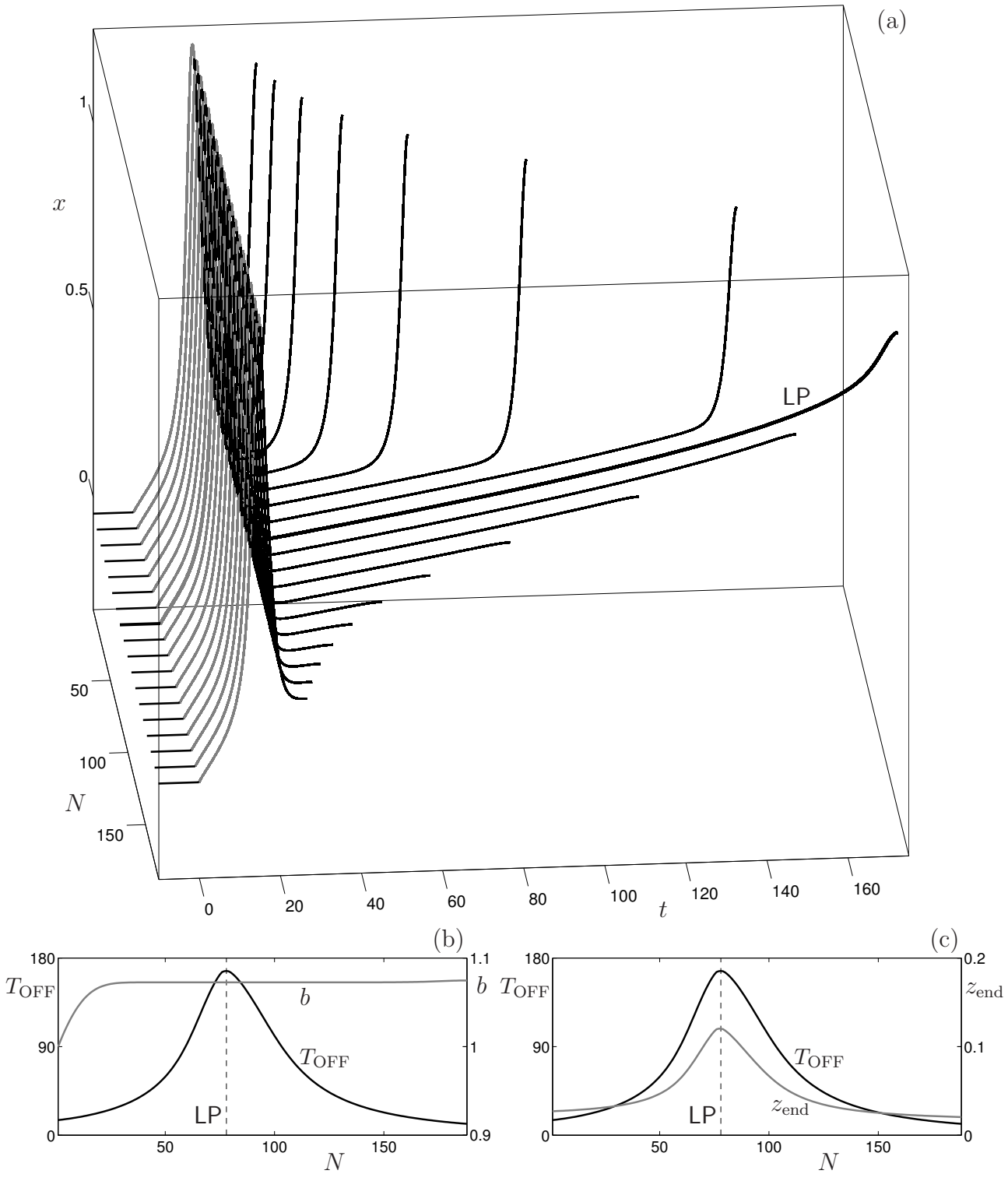

Figure 7: Deformation of an orbit segment pair $(\mathbf{u}_{\rm ON}, \mathbf{u}_{\rm OFF})$ through the moment of the second spike onset. Here, $h = 1$ is fixed and $b = 1$ at the start of the continuation. Note how the end point transforms from a local maximum into a local minimum, which is detected as a fold bifurcation. Panel (a) shows a waterfall diagram of the orbit segments computed as part of the continuation; panel (b) shows the variation of $T_{\rm OFF}$ (black) and b (grey), while panel (c) plots $T_{\rm OFF}$ (black) and z (grey) as a function of N. The spike onset is detected at LP.

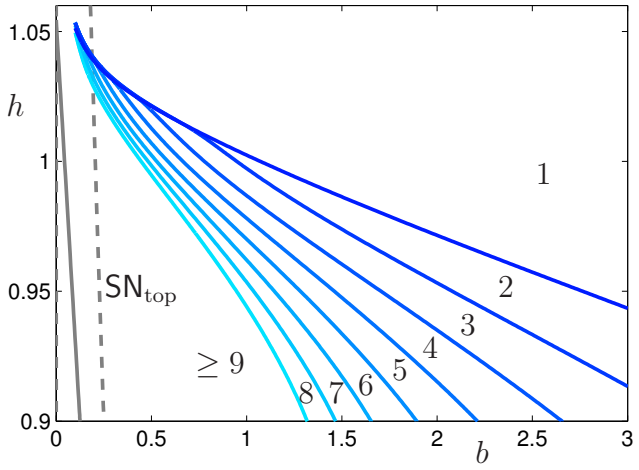

Figure 8: Two-parameter bifurcation diagram indicating the regions in the (b, h)-plane with different numbers of additional spikes.

the saddle-node bifurcation curve SN_{top} before reaching this value. Two additional equilibria exist in the region to the left of SN_{top} and the response is influenced by the existence of a (perturbation-induced) heteroclinic connection from FP to a different equilibrium of saddle type; the effect of this heteroclinic connection on the bifurcation diagram is beyond the scope of this paper. In particular, the computed curves all accumulate in this region, but we did not further pursue the investigation of the possible existence of an accumulation point near $b = 0.1$.

The (b, h)-parameter bifurcation diagram is very similar to the two-parameter bifurcation diagram computed for the model in [22]. This is perhaps not surprising, because system (1) has the same qualitative behaviour. Furthermore, the parameters b and h can be viewed as conductances, which were the parameters varied in [22]. As h decreases, the curves of spike onset fan out and form well-defined regions inside which the numbers of spikes in the transient response are constant. For b and h both large, the system immeditately relaxes back to FP without producing additional spikes. As b decreases, we successively cross bifurcation curves that correspond to the onset of an additional spike in the transient burst. We refer back to the responses shown in Figures 3 and 4. The response in Figure 3 corresponds to the point $(b, h) = (0.75, 1)$ in Figure 8, which is exactly in the regime where we expect to see a transient burst with four spikes. Similarly the responses in Figure 4(b)-(e) correspond to points $(b, h) = (1.15, 1)$, $(b, h) = (1.0, 1)$, $(b, h) = (0.85, 1)$, and $(b, h) = (0.43, 1)$ in Figure 8, which lie, as expected, in the regimes for one, two, three, and at least nine spikes, respectively.

We remark here that the computation of curves of spike onset is more efficient than a two-parameter brute-force simulation approach to determine the regions inside which the transient bursts have an equal number of spikes. Furthermore, as h increases, these curves accumulate and a brute-force method will have difficulty determining the region boundaries. Our continuation method does not have this problem, because the solution pairs $(\mathbf{u}_{\text{ON}}, \mathbf{u}_{\text{OFF}})$ for different spike numbers are well separated in phase space, so that the two-point BVP continuation is not affected by the parameter accumulation.

5 Discussion

In this paper, we analysed transient dynamics arising due to a brief perturbation from equilibrium state in a generic (polynomial) bursting cell model. We focussed on the transient bursting behaviour following a short-time current injection. In our analysis, we utilised the separation of time scales in the system. The spike-adding process is characterised by the fact that orbit segments trace the slow manifold of saddle type associated with the saddle branch of the Z-shaped family of equilibria for the fast subsystem. We obtained an approximation of the local stable manifold of this saddle slow manifold by computing the family of one-dimensional stable manifolds of the fast subsystem; we showed that a spike-adding transition is organised by this family and the branch of saddle equilibria in the fast subsystem.

We have previously shown that such invariant objects are responsible for the spike-adding transition in a five-dimensional pyramidal neurone model [21]. The analysis presented in this paper demonstrates that spike adding in a transient burst can already occur in a three-dimensional system with one slow and two fast variables. Hence, our three-dimensional generic model system is an ideal low-dimensional model for further research into the mechanisms of transient bursting dynamics, which offers qualitative insight into transient bursting for higher-dimensional detailed neuronal models.

Based on our earlier work [22], the onset of a new spike coincides with a maximum in the time T_{OFF}, but such a maximum is accompanied by an extremum in the slow variables of the model. This means that the onset of a new spike can be detected as a fold bifurcation with respect to this intrinsically bounded slow variable. With the present study we confirm our conjecture and use fold detection and continuation with respect to the slow variable z in a suitable two-parameter boundary value problem to compute the curves of spike onset in a two-parameter plane. For our three-dimensional generic model system, the parameter value at which the system exhibits a local maximum in z is indistinguishable from the value at which it achieves a local maximum in the associated integration time.

We note the similarities between spike adding for periodic bursting and spike adding in a transient burst in regard to mechanisms (key model parameters) that control the number of spikes within a burst. We show that the number of spikes in a transient burst depends on the parameter b that couples the dynamics of the slow variable z to the fast subsystem dynamics in the model. Interestingly, a decrease in this parameter decreases the number of spikes in the transient burst (Figure 8), in accordance with the effect that a decrease in b has on the number of spikes in the periodic bursting regime (unpublished observations). Since b could roughly be interpreted as proportional to the large-conductance calcium-activated potassium (BK) current, the effect of blocking this channel (i.e., decreasing b) on the number of spikes (or the duration of the active phase) in the case of periodic bursting [19, 32] is also consistent with the results presented in this paper.

The (b, h)-parameter diagram shown in Figure 8 corresponds to a short-current application with amplitude $I_{\mathrm{app}} = 0.02$ and duration $T_{\mathrm{ON}} = 15$. The choice for I_{app} and T_{ON} determines how the response is perturbed away from the full-system equilibrium FP. These parameters must be such that a first spike is triggered; otherwise,

the transient response exhibits no bursts at all. In particular, $I_{\rm app}$ should be large enough. On the other hand, we are interested in the intrisic bursting behaviour of (1) and the applied current should give rise to no more than one spike. This means that it is best to choose $T_{\rm ON}$ as small as possible for any given $I_{\rm app}$. Despite these constraints, $I_{\rm app}$ and $T_{\rm ON}$ can be varied, and one may wonder how this affects the (b,h)-parameter diagram, or other parameter variation. Indeed, the position $\mathbf{u}_{\rm ON}(1)$ in phase space as the applied current is switched off controls the number of spikes in the transient burst. However, we find that $\mathbf{u}_{\rm ON}(1)$ hardly changes as b and h vary. Hence, the variation in the number of spikes for the (b,h)-parameter diagram is primarily determined by the relative changes of the invariant manifolds in the fast subsystem of (1), which are independent of $I_{\rm app}$ and $T_{\rm ON}$. This means that any curve of spike onset depends continuously on $I_{\rm app}$ and $T_{\rm ON}$ and the (b,h)-parameter diagram will change only qualitatively with small variations of $I_{\rm app}$ and/or $T_{\rm ON}$.

We limited our analysis to the case of spike adding in a transient burst when there are no additional equilibria present in the unperturbed system. An investigation of all possibilities remains an interesting and challenging project for future work.

Acknowledgements. We would like to thank the World-wide Universities Network scheme for facilitating our collaboration through research visits to the University of Bristol and The University of Auckland, respectively. The research of HMO was supported by grant UOA1113 of the Royal Society of New Zealand Marsden Fund. The research of KT-A was supported by grant EP/I018638/1 of the Engineering and Physical Sciences Research Council (EPSRC) and by AlterEgo, a project funded by the European Union grant #600610.

References

[1] P. Andersen, R. Morris, D. Amaral, T. Bliss, and J. O'Keefe, *The Hippocampus Book* (Oxford University Press, New York, 2007).

[2] S.M. Baer, T. Erneux, and J. Rinzel, The slow passage through a Hopf bifurcation: Delay, memory effects, and resonance, *SIAM J. Appl. Math.* **49**(1), 55–71 (1989).

[3] J.T. Brown, J. Chin, S.C. Leiser, M.N. Pangalos, and A.D. Randall. Altered intrinsic neuronal excitability and reduced Na+ currents in a mouse model of alzheimer's disease. *Neurobiology of Aging*, **32**(11), 2109–2114 (2011).

[4] J.T. Brown and A.D. Randall. Activity-dependent depression of the spike after-depolarization generates long-lasting intrinsic plasticity in hippocampal CA3 pyramidal neurons. *The Journal of Physiology*, **587**(6), 1265–1281 (2009).

[5] D. Bucher and J.M. Goaillard. Beyond faithful conduction: short-term dynamics, neuromodulation, and long-term regulation of spike propagation in the axon. *Progress in Neurobiology*, **94**(4), 307–346 (2011).

[6] M. Desroches, J. Guckenheimer, B. Krauskopf, C. Kuehn, H.M. Osinga, and M. Wechselberger, Mixed-mode oscillations with multiple time scales, *SIAM Review* **54**(2), 211–288 (2012).

[7] M. Diener, The canard unchained or how fast/slow dynamical systems bifurcate, *The Mathematical Intelligencer* **6**, 38–48 (1984).

[8] E.J. Doedel, AUTO: A program for the automatic bifurcation analysis of autonomous systems, *Congressus Numerantium* **30**, 265–284 (1981).

[9] E.J. Doedel and B.E. Oldeman, with major contributions from A.R. Champneys, F. Dercole, T.F. Fairgrieve, Yu.A. Kuznetsov, R.C. Paffenroth, B. Sandstede, X.J. Wang and C.H. Zhang, AUTO-07p: Continuation and bifurcation software for ordinary differential equations, Concordia University, Montreal, Canada; available from `http://cmvl.cs.concordia.ca/auto/` (2007).

[10] F. Dumortier and R. Roussarie, *Canard cycles and center manifolds*, Mem. Amer. Math. Soc. **121** (1996); with an appendix by Cheng Zhi Li.

[11] G.B. Ermentrout and D.H. Terman, *Mathematical Foundations of Neuroscience* (Springer-Verlag, New York, 2010).

[12] W. Govaerts, and A. Dhooge, Bifurcation, bursting and spike generation in a neural model, *Int. J. Bifurcation and Chaos* **12**(8), 1731–1741 (2002).

[13] J. Guckenheimer, S. Gueron, and R.M. Harris-Warrick, Mapping the dynamics of a bursting neuron, *Philos Trans R Soc Lond, B, Biol Sci* **341**(1298), 345–59 (1993).

[14] J. Guckenheimer and C. Kuehn, Computing slow manifolds of saddle type, *SIAM J. Appl. Dyn. Sys.* **8**(3), 854–879 (2009).

[15] J. Guckenheimer, J.H. Tien, and A.R. Willms, Bifurcations in the fast dynamics of neurons: implications for bursting, in S. Coombes and P.C. Bressloff (Eds.) *Bursting: The Genesis of Rhythm in the Nervous System*, pp. 89–122 (World Scientific Publishing, Singapore, 2005).

[16] J.L. Hindmarsh and R.M. Rose, A model of neuronal bursting using 3 coupled 1st order differential-equations, *Proc. Royal Soc. London Series B — Biological Sciences* **221**(1222), 87–102 (1984).

[17] B. Krauskopf and H. M. Osinga, Computing invariant manifolds via the continuation of orbit segments, in B. Krauskopf, H. M. Osinga and J. Galán-Vioque (Eds.) *Numerical Continuation Methods for Dynamical Systems*, Underst. Complex Syst., pp. 117–154 (Springer-Verlag, New York, 2007).

[18] Yu.A. Kuznetsov, *Elements of applied bifurcation theory.* (Springer-Verlag, New York, 1998).

[19] J. Nowacki, S. H. Mazlan, H. M. Osinga, and K. T. Tsaneva-Atanasova. The role of large-conductance calcium-activated K^+ (BK) channels in shaping bursting oscillations of a somatotroph cell model. *Physica D*, **239**(9), 485–493 (2010).

[20] J. Nowacki, H.M. Osinga, J.T. Brown, A.D. Randall, and K.T. Tsaneva-Atanasova, A unified model of CA1/3 pyramidal cells: An investigation into excitability, *Progr. Biophysics and Molecular Biology* **105**(1-2), 34–48 (2011).

[21] J. Nowacki, H.M. Osinga, and K.T. Tsaneva-Atanasova, Dynamical systems analysis of spike-adding mechanisms in transient bursts, *J. Mathematical Neuroscience* **2**, 7 (2012).

[22] J. Nowacki, H.M. Osinga, and K.T. Tsaneva-Atanasova, Continuation-based numerical detection of after-depolarisation and spike-adding threshold, *Neural Computation* **25**(4), 877–900 (2013).

[23] H.M. Osinga, A. Sherman, and K.T. Tsaneva-Atanasova, Cross-currents between biology and mathematics: The codimension of pseudo-plateau bursting, *Discrete and Continuous Dynamical Systems – Series A* **32**(8), 2853–2877 (2012).

[24] H.M. Osinga and K.T. Tsaneva-Atanasova, Dynamics of plateau bursting depending on the location of its equilibrium, *J. Neuroendocrinology* **22**(12), 1301–14 (2010).

[25] J. Rinzel, Bursting oscillations in an excitable membrane model, in B.D. Sleeman and R.J. Jarvis (Eds.) *Ordinary and Partial Differential Equations (Dundee, 1984)*, Lecture Notes in Math., vol. 1151, pp. 304–316 (Springer-Verlag, New York, 1985).

[26] J. Rinzel, A formal classification of bursting mechanisms in excitable systems, in A.M. Gleason (Ed.) *Proc. Int. Congress Math., Berkeley 1986*, vol 1, 2, pp. 1578–1593 (Amer. Math. Soc., Providence, RI, 1987); also (with slight differences) in E. Teramoto and M. Yamaguti (Eds.) *Mathematical Topics in Population Biology, Morphogenesis and Neuroscience*, Lecture Notes in Biomath., vol. 71, pp. 267–281 (Springer-Verlag, Berlin, 1987).

[27] A. Shilnikov and M. Kolomiets, Methods of the qualitative theory for the Hindmarsh-Rose model: A case study. A tutorial, *International Journal of Bifurcation and Chaos* **18**(8), 2141–2168 (2008).

[28] M. Storace, D. Linaro, and E. de Lange, The Hindmarsh-Rose neuron model: Bifurcation analysis and piecewise-linear approximations, *CHAOS* **18**, 033128 (2008).

[29] D.H. Terman, Chaotic spikes arising from a model of bursting in excitable membranes, *SIAM J. Appl. Math.* **51**(5), 1418–1450 (1991).

[30] D.H. Terman, The transition from bursting to continuous spiking in excitable membrane models, *J. Nonlinear Science* **2**(2), 135–182 (1992).

[31] K.T. Tsaneva-Atanasova, H.M. Osinga, T. Rieß, and A. Sherman, Full system bifurcation analysis of endocrine bursting models, *J. Theoretical Biology* **264**(4), 1133–1146 (2010).

[32] K. Tsaneva-Atanasova, A. Sherman, F. van Goor and S. S. Stojilkovic, Mechanism of spontaneous and receptor-controlled electrical activity in pituitary somatotrophs: Experiments and theory, *J. Neurophysiology*, **98**, 131–144 (2007).